INSTITUTE OF PHYSICS PUBLISHING JOURNAL OF PHYSICS B: ATOMIC, MOLECULAR AND OPTICAL PHYSICS

J. Phys. B: At. Mol. Opt. Phys. **37** (2004) L235–L242 PII: S0953-4075(04)77190-4

**LETTER TO THE EDITOR**

# Photoelectron–photoion–photoion coincidence in Ar dimers

**A De Fanis[1,2], M Oura[3], N Saito[4], M Machida[3,5], M Nagoshi[5], A Knapp[6], J Nickles[6], A Czasch[6], R Dörner[6], Y Tamenori[1], H Chiba[2], M Takahashi[2], J H D Eland[2,7] and K Ueda[2]**

[1] Japan Synchrotron Radiation Research Institute, Sayo, Hyogo 679-5198, Japan
[2] Institute of Multidisciplinary Research for Advanced Materials, Tohoku University, Sendai 980-8577, Japan
[3] RIKEN, Harima Institute, 1-1-1 Kouto, Mikazuki, Sayo, Hyogo 679-5198, Japan
[4] National Metrology Institute of Japan, AIST, Tsukuba 305-8568, Japan
[5] Department of Material Science, Himeji Institute of Technology, Kamigori 678-1297, Japan
[6] Universität Frankfurt, Institut für Kernphysik, D-60486 Frankfurt, Germany
[7] PTCL, Oxford University, Oxford, UK

E-mail: ueda@tagen.tohoku.ac.jp

Received 8 March 2004
Published 27 May 2004
Online at stacks.iop.org/JPhysB/37/L235
DOI: 10.1088/0953-4075/37/12/L01

**Abstract**

Photoelectron–photoion–photoion coincidence momentum imaging was applied to study 2p photoemission from Ar dimers. We present measurements of the kinetic energy released in fragmentation of $Ar_2^{++}$, angular distributions of energetic fragments, angular distributions of photoelectrons in the laboratory frame and in the molecular frame. The mean kinetic energy of fragment $Ar^+$ ions, 2.2 eV, is larger than the value estimated from the Coulomb explosion model with the equilibrium Ar–Ar distance. No significant differences between the photoelectron angular distributions of monomers and dimers can be found in the laboratory frame. The photoelectron angular distributions of dimers in the molecular frame show a minimum for electron emission along the dimer axis at low energies (1.2 and 3.4 eV) and become isotropic at higher kinetic energies.

Coincidence momentum imaging has progressed greatly in the last few years and can now reveal a great deal of information in molecular electron spectroscopy. It is especially effective when combined with sources of monochromatic tunable and polarized radiation, obtained at VUV–soft x-ray beamlines of modern synchrotron light sources. A light atom in a molecule with an inner-shell vacancy decays by Auger emission after a delay of the order

  

of femtoseconds. The multiply charged parent molecular ion thus produced often fragments by Coulomb explosion. Multiple coincidence momentum imaging of the fragment ions makes it possible to access information which cannot be revealed in experiments where only one particle is detected. Indeed, momentum vector correlations measured by coincidence momentum imaging reveal the nuclear motion and molecular deformation specific to each symmetry of the excited and/or ionized state [1, 2, 3]. If the photoelectron momentum is measured in coincidence with the ion momentum, one can study photoemission from a specific shell to a continuum orbital of defined symmetry, within the molecular frame [4, 5–8].

Electron–multiple ion coincidence momentum imaging has so far been applied successfully to simple stable molecules such as $N_2$, CO [5, 6] and $CO_2$ [7, 8] but not yet to small clusters. In order to study photoemission from clusters of a certain size one must extract the corresponding signal, which is in general embedded in large signals due to monomers and mixed with signals from clusters of different sizes. We report on the first experiment for inner-shell photoemission from size-selected clusters. Although the results reported here are only for 2p photoemission from Ar dimers, we emphasize that the coincidence imaging provides a powerful and unique tool to study inner-shell photoemission of size-selected clusters in both the laboratory and molecular reference frames.

The experiment was performed at the c-branch of beamline 27SU [9, 10] at SPring-8, the 8-GeV synchrotron facility in Japan, with the same apparatus and technique as described earlier [7, 8]. A vertical supersonic gas-jet enters the interaction region where it crosses the horizontal photon beam. Electrons and fragment ions are driven to either side by a uniform electrostatic field. At one end of the interaction region, ions are detected by a set of micro-channel plates (MCP) of 80 mm in diameter. On the other side, electrons enter a field-free drift tube and are detected by a similar MCP at its end. The distance between the source point and the MCP for ion detection is 21.5 mm, whereas the distance between the source point and the entrance of the drift tube is 70 mm. The length of the drift tube is 140 mm so that Wiley–McLaren focusing conditions are ensured. A uniform magnetic field is superimposed on the spectrometer by a set of Helmholtz coils outside the vacuum chamber, to help in driving the electrons onto the MCP. A delay line anode at the rear of each MCP allows us to extract the position and time of hit of each particle. From the position and time, $(x, y, t)$, one can extract information about the three-dimensional momentum vector, $(px, py, pz)$, in the laboratory frame by off-line analysis.

We present measurements recorded at photon energies of 252.0, 264.3 and 294.9 eV. The lower values of the photon energy were known by calibrating the monochromator scale with the Ar 2p resonances [11]. The higher value of 294.9 eV was set by tuning the photon energy on the $CO_2$ C $1s^{-1}$ 3p resonance [12]. The binding energies of the $2p_{1/2}$ and $2p_{3/2}$ orbitals investigated here are 250.8 and 248.6 eV, respectively [11].

For the lowest energy, where the 2p photoelectrons have energies of 1.2 and 3.4 eV, the electric and magnetic fields were 600 V $m^{-1}$ and 3.6 G; these were increased to 1200 V $m^{-1}$ and 9.7 G for the intermediate electron energy of 15 eV, and to 2700 V $m^{-1}$ and 16 G for the experiment with electron energy of 46 eV. The time spread for photoelectrons varies from 20 to 35 ns and for fragment ions its range is 1.1–4.6 $\mu$s. The spatial and time resolutions of the detectors are about 1 mm and 0.5 ns, the consequent energy resolutions for photoelectrons were 1, 6 and 14 eV with a peak height to background ratio of 1:10 or better. The direction of linear polarization of the synchrotron radiation is vertical for experiments with photon energies of 252.0 and 264.3 eV; at the highest energy of 294.9 eV, the data were recorded in two separate runs with directions of polarization vertical and horizontal, respectively.

The cluster jet was created by supersonic expansion of Ar gas. The gas sample exits a nozzle with a pin-hole of 30 $\mu$m diameter, 7 mm distant from a skimmer of 300 $\mu$m

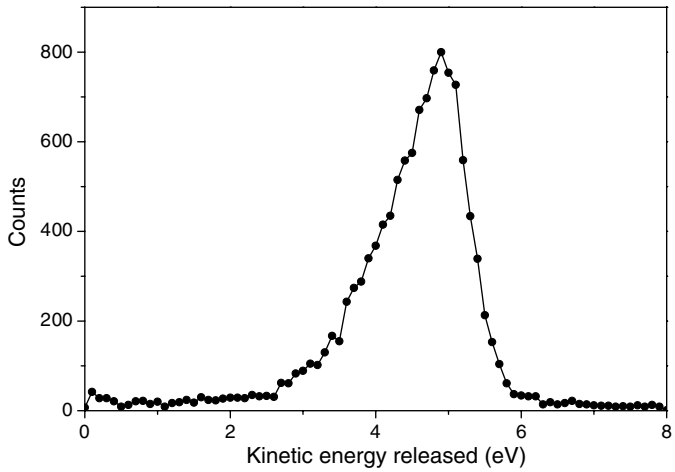


**Figure 1.** Measured distribution of kinetic energy released by $Ar^+$–$Ar^+$ Coulomb explosion, recorded at a photon energy of 294.9 eV.

diameter. The skimmer is 45 mm below the ionization region in the main chamber. The stagnation pressure of the gas was 2.6 bar, while the pressure in the vacuum chamber housing the spectrometer was of the order of $10^{-7}$ mbar. The gas source was not constructed with the purpose of studying clusters and the only parameters that could be adjusted to favour the creation of clusters were the distance between nozzle and skimmer and the stagnation pressure. The ratio of clusters to monomers was less than 1:100. As a result, most ionization events create a photoelectron and a singly charged ion which immediately becomes doubly charged by Auger emission. The fields and geometry of the spectrometer are such that most Auger electrons are not collected. The doubly charged ions created by photoemission and Auger decay have no kinetic energy and end up at the centre of the detector. The resulting high count rate on a small area can damage the MCP and cause false coincidence counts.

A small fraction of the total beam is in the form of dimers or larger clusters. After emission of a 2p photoelectron, the $Ar_2^+$ singly charged dimer can decay to $Ar_2^{++}$ by normal Auger emission. Immediately after the Auger process has occurred, the doubly charged ion fragments by Coulomb explosion and two $Ar^+$ ions are detected. These $Ar^+$ ions resulting from initial dimers must be extracted from the whole set of counts containing a large majority of $Ar^{++}$ ions produced from monomers or clusters. First, only events containing at least one electron and two ions within 10 $\mu$s are accepted by a gated electronic coincidence unit and are fed into the acquisition board. Then, the events are processed by software. The time-of-flight (TOF) of $Ar^{++}$ is a sharp distribution peaked at 3900, 2900 and 2100 ns with widths of 70, 45 and 35 ns under the three sets of experimental conditions, whereas the TOF of $Ar^+$ fragments is distributed over 3700–8500, 3000–5600 and 2400–3600 ns. Thus, $Ar^{++}$ can be eliminated by imposing an acceptance window on the TOF of the ion detected. This is however insufficient to discriminate against $Ar^+$ created from sources other than fragmentation of $Ar^+$–$Ar^+$, or against ion counts from background gas. These unwanted counts are still more numerous than those of interest. The procedure to select only the counts corresponding to $Ar^+$ from fragmentation of $Ar^+$–$Ar^+$ is to impose, in off-line analysis, an acceptance window on the sum of the momentum of the two ions, using the momentum conservation law. This selection also rejects ion counts resulting from explosion of larger clusters.

Figure 1 presents the distribution of kinetic energy released (KER) from the $Ar^+$–$Ar^+$ Coulomb explosions. We show only the data measured at the photon energy of 294.9 eV, as

the distributions measured at other energies are almost identical. This lack of photon energy dependence is not surprising, because the KER is a consequence of the $Ar^+$–$Ar^+$ Coulomb repulsion at a definite internuclear distance, which can be expected to be similar to the Ar–Ar equilibrium distance. Calculated equilibrium bond lengths Ar–Ar range between 3.76 and 4.06 Å [13]. Coulomb repulsion between two ions at these distances should result in a KER between 3.84 and 3.55 eV. The weighted average of the measured KER distribution, 4.4 eV, is thus rather larger than estimated. We do not know the reason of the discrepancy between measured and calculated KER distributions. Contaminations from larger clusters cannot be the reason for this discrepancy: in two-dimensional distribution of TOF of first fragment versus TOF of the second fragment (PIPICO spectrum), a very narrow line corresponds to the $Ar^+$–$Ar^+$ coincidence resulting from Ar dimers. The existence of larger clusters would result in such a narrow line being superimposed on a very broad one, which is actually absent. Furthermore, if larger clusters existed they would be discriminated by imposing the momentum conservation law for two fragments. In a different experiment (unreported) we measured the KER for the $CO_2 + h\nu \rightarrow O^+ + CO^+$ fragmentation, which peaks at about 6 eV; but the equilibrium bond length of C–O is 1.164 Å, suggesting the Coulomb explosion energy of 8.2 eV. The experimental value of 6 eV is however very close to the previous experimental value of [14].

The KER distribution is calculated from the experimental data by using ions emitted over $4\pi$, thus by using a combination of both TOF and position of hit on the MCP. If we select ions emitted towards the detector, or perpendicular to it, only either the TOF or the position of hit determines the extracted KER. Within these selections, we always obtain KER distribution consistent with that presented in figure 1. Thus, we have confidence in the reliability of the present measurement.

The great majority of ion counts are from non-energetic $Ar^{++}$ which arrive near the centre of the MCP. Eventually, this damages the detector by burning the MCP near its centre, where it becomes less efficient. As a consequence, angular distributions of energetic fragments in the dipole plane, the plane perpendicular to the radiation propagation direction, could not be measured. It was however possible to extract the angular distribution of energetic fragments ejected in the plane parallel to the MCP, because fragments ejected in such a plane hit the MCP far from its centre, where the damage does not occur. This angular distribution is found to be isotropic at all energies.

Figure 2 exhibits the 2p photoelectron spectra of Ar dimers and monomers, measured at the photon energy of 252.0 eV. The two bands at 1.2 and 3.4 eV correspond to the $2p_{1/2}$ and $2p_{3/2}$ components, respectively. It is clear from the figure that with the present resolution the energies of the 2p photoelectrons from dimers and monomers coincide. The structure in the photoelectron spectrum of dimers is narrower than in the case of monomers. This is a consequence of the discrimination imposed by the software analysis: by requiring the momentum conservation law for the two fragments a smaller interaction region is automatically selected, this discriminates on part of the background and enhances the energy resolution. At higher energies the doublet structure is no longer resolved.

From measurements of the photoelectron momentum in the laboratory frame one can extract the asymmetry parameter that describes the angular distribution of photoelectrons. Figure 3 shows the angular distributions of 2p photoelectrons from monomers and dimers in the dipole plane, measured at the photon energy of 264.3 eV. The figure also includes least-squares fits to second-order Legendre polynomials to extract the values of $\beta$. The angular distribution of 2p photoelectrons from Ar monomers is investigated here only as a check of consistency with previous measurements. Values of $\beta$ extracted from the present measurements for both dimers and monomers are presented in table 1, together with the

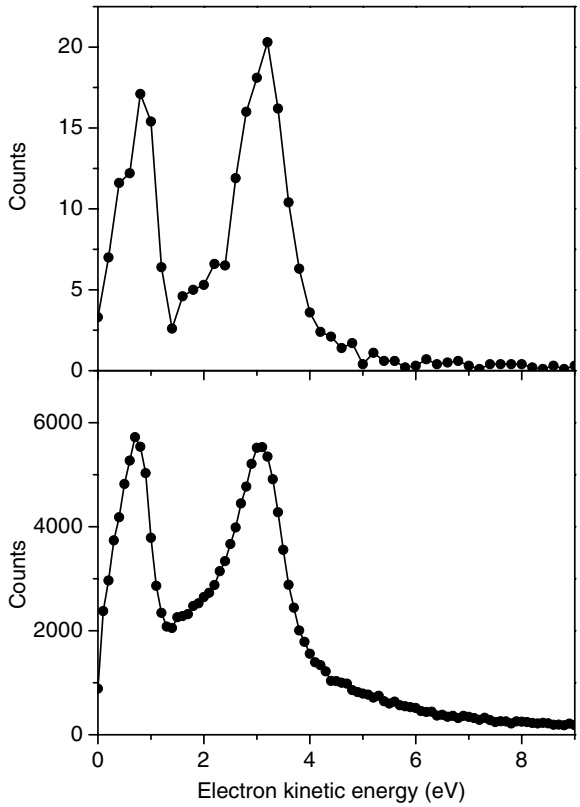


**Figure 2.** 2p photoelectron spectra of Ar dimers (upper) and monomers (lower) recorded at the photon energy of 252.0 eV.

**Table 1.** Values of $\beta$ extracted from the present measurements, compared to known values from conventional photoelectron spectroscopy.

| $h\nu$ | | Kinetic energy | $\beta$ | | |
|---|---|---|---|---|---|
| (eV) | $j$ | (eV) | Dimer | Monomer | |
| 252.0 | 1/2 | 1.2 | 0.6 | 0.7 | 0.65 [16] |
| | 3/2 | 3.4 | 0.8 | 0.6 | 0.25 [16] |
| 264.3 | Unresolved | 15 | 0.6 | 0.7 | 0.35 [16] |
| 294.9 | Unresolved | 46 | 0.8 | 0.5 | 0.8 [15] |

published values [15, 16]. We estimate the uncertainties of the present $\beta$ values to be $\pm 0.3$ or better; these relatively large uncertainties arise from spatial and temporal non-uniformity of the fields. Within these uncertainties, the $\beta$ values for Ar 2p photoelectrons of dimers and monomers do not exhibit significant differences.

From measurements of the momentum vector of each particle detected in coincidence, one can extract the direction of electron emission in the molecular frame defined by the dimer axis, as in the case of linear molecules [5–8]. From these data, photoelectron angular distributions (PADs) in the molecular frame, averaged over the polarization directions, are constructed in the following way. First a finite set of planes in the laboratory frame is defined by the analysis

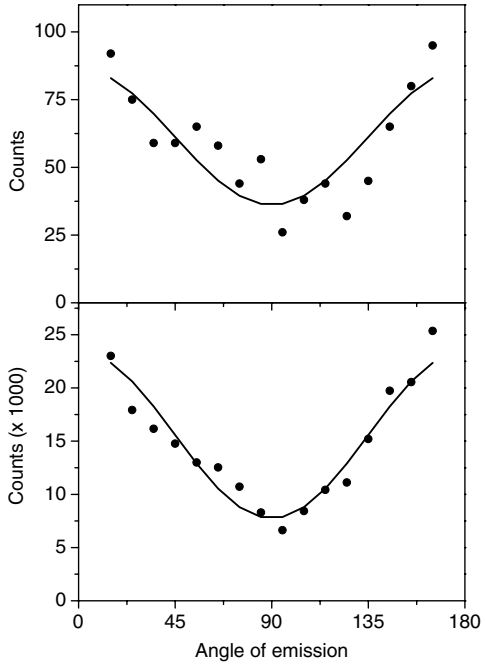


**Figure 3.** Angular distribution of 2p photoelectrons in the dipole plane ($\pm 10^\circ$) from Ar dimers (upper) and monomers (lower) at the photon energy of 264.3 eV. The angle is measured from the direction of polarization of the radiation. Points: measurements, line: least-squares fit with a second-order Legendre polynomial.

software, equally separated by $40^\circ$ and all containing the polarization direction. If both the dimer axis and the electron momentum in the coincidence event are contained within one of these planes ($\pm 20^\circ$), the event is included in the construction of PADs. On each plane, we measured the PAD in the body frame (relative to the dimer axis), specifying the dimer axis relative to the polarization direction, and then sum over all the directions of polarization. This integration over the direction of polarization is chosen as it makes it possible to use a large fraction of all coincidence data, but it also removes the effect of the polarization direction. The resulting PAD reflects exclusively the influence of the dimer environment on the photoelectron, if any. The PAD constructed in this way could still be affected by the non-uniform detection efficiency of the ion MCP due to the high count rates of $Ar^{++}$ from monomers. This unwanted effect is absent when the fragments are emitted almost parallel to the MCP plane, perpendicular to the TOF axis, and hit the MCP far from its centre, but it becomes very severe in the plane that includes the TOF axis. This experimental artefact was compensated by rescaling the coincidence counts, assuming the ion angular distribution to be uniform in all planes. The PADs constructed in this way are presented in figures 4(a) and (b), measured at a single photon energy of 252.0 eV and showing the $2p_{1/2}$ and $2p_{3/2}$ components at kinetic energies of 1.2 and 3.4 eV (see figure 2). Parts (c) and (d) of the figure are measured at photon energies of 264.3 and 294.9 eV, 15 and 46 eV above the 2p threshold, where the spin–orbit components are not resolved. The data at 46 eV are from two separate runs with vertical and horizontal polarizations respectively; both are included in figure 4(d). The expected symmetry properties that the four quadrants of $90^\circ$ extension are identical have been imposed on all the PADs presented here. The data at the two lowest energies show lower

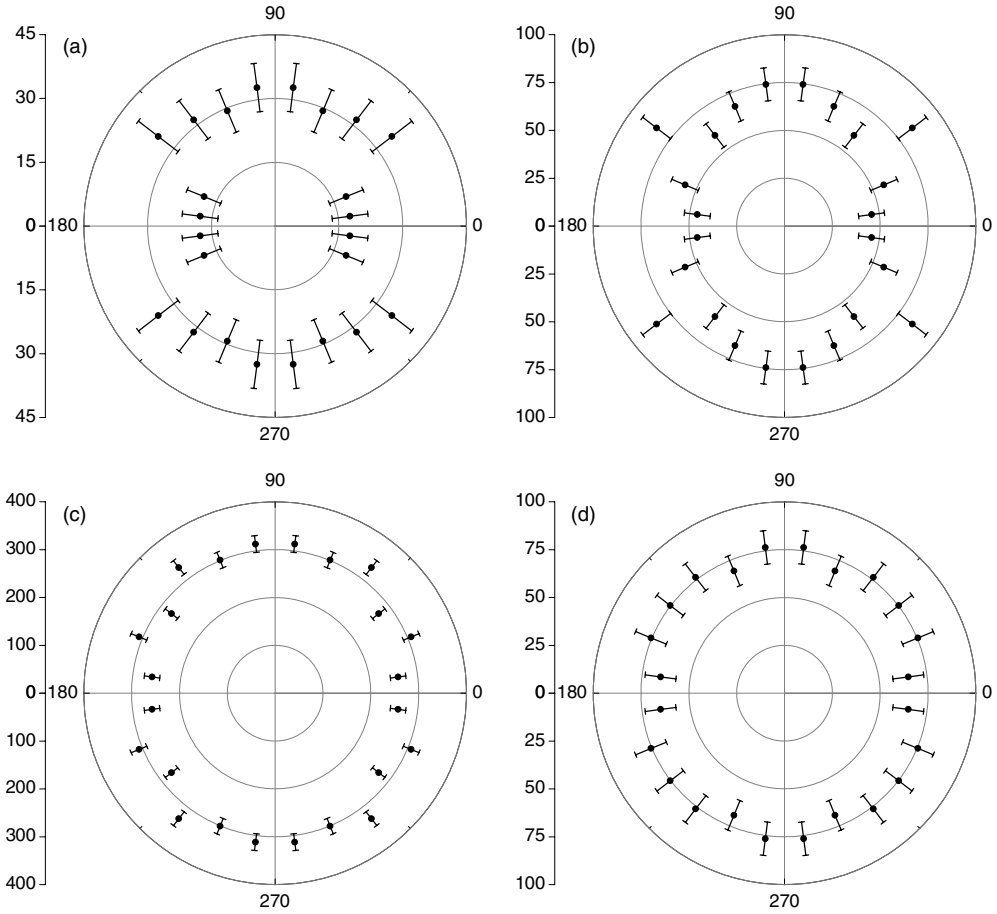


**Figure 4.** Angular distribution of 2p photoelectrons in the dimer body frame: (a) and (b) are recorded at the photon energy of 252.0 and present the $2p_{1/2}$ and $2p_{3/2}$ components, at excess energies of 1.2 and 3.4 eV, respectively; (c) and (d) are recorded at 264.3 and 294.9 eV, 15 and 46 eV above the 2p threshold. The dimer axis is horizontal, the vertical scale represents counts.

intensity for electron emission along the dimer axis, which could be interpreted as destructive interference from the electron waves scattered by the dimer environment. In fact, also in other situations the interference between partial wave components of different symmetries is responsible for non-isotropic angular distribution of photoelectrons in the molecular frame [4, 5, 8, 17]; though in these works the symmetry of the sample molecule is specified by the detection of fragments emitted in a given direction. The PADs at 15 and 46 eV, on the other hand, present rather isotropic electron emission in the body frame.

In conclusion, we have reported the first experiment on photoelectron–photoion–photoion coincidence momentum imaging from a cluster. The angular distribution of energetic fragment ions is isotropic. We found no significant difference between the angular distributions of Ar 2p photoelectrons from monomers or dimers. The PADs in the body frame are anisotropic near threshold and become isotropic at higher energies. We emphasize that the coincidence momentum imaging provides a powerful and unique tool to study inner-shell photoemission of size-selected clusters both in the laboratory and body frames.

## Acknowledgments

This experiment was carried out with the approval of the SPring-8 program review committee and partly supported by grants in aid from JSPS. This work was partly supported by the Grants-in-Aid for Scientific Research (B) from Japan Society for Promotion of Science and by the Budget for Nuclear Research of Ministry of Education, Culture, Sports, Science and Technology, based on the screening and counselling by the Atomic Energy Commission. The Frankfurt collaborators acknowledge support by DFG and BMBF; AK thanks Graduiertenförderung des Landes Hessen for financial support. We are grateful to the staff at SPring-8 for their help.

## References

[1] Muramatsu Y *et al* 2002 *Phys. Rev. Lett.* **88** 133002
[2] Ueda K *et al* 2003 *Chem. Phys.* **289** 135
[3] De Fanis A, Saito N, Machida M, Okada K, Chiba H, Cassimi A, Dörner R, Koyano I and Ueda K 2004 *Phys. Rev.* A **69** 022506
[4] Shigemasa E, Adachi J, Oura M and Yagishita A 1995 *Phys. Rev. Lett.* **74** 359
[5] Landers A *et al* 2001 *Phys. Rev. Lett.* **87** 013002
[6] Weber T *et al* 2001 *J. Phys. B: At. Mol. Opt. Phys.* **34** 3669
[7] De Fanis A *et al* 2002 *Phys. Rev. Lett.* **89** 023006
[8] Saito N *et al* 2003 *J. Phys. B: At. Mol. Opt. Phys.* **36** L25
[9] Ohashi H *et al* 2001 *Nucl. Instrum. Methods* A **467–468** 533
[10] Ohashi H, Ishiguro E, Tamenori Y, Kishimoto H, Tanaka M, Irie M and Ishikawa T 2001 *Nucl. Instrum. Methods* A **467–468** 529
[11] King G C, Tronc M, Read F H and Bradford R C 1977 *J. Phys. B: At. Mol. Phys.* **10** 2479
[12] Prince K, Avaldi L, Coreno M, Camilloni R and de Simone M 1999 *J. Phys. B: At. Mol. Opt. Phys.* **32** 2551
[13] Slavíček P, Kalus R, Paska P, Odvárková I, Hobza P and Malijevský A 2003 *J. Chem. Phys.* **119** 2102
[14] Heiser F, Saito N and Becker U unpublished data
[15] Lindle D W, Medhurst L J, Ferrett T A, Heimann P A, Liu S H, Shirley D A, Carlson T A, Deshmukh P C, Nasreen G and Manson S T 1988 *Phys. Rev.* A **38** 2371
[16] Avaldi L, Dawber G, Camilloni R, King G C, Roper M, Siggel M R F, Stefani G and Zitnik M 1994 *J. Phys. B: At. Mol. Opt. Phys.* **27** 3953
[17] Avaldi M and Briggs J 1999 *J. Phys. B: At. Mol. Opt. Phys.* **32** 2487